

CRUSTAL DYNAMICS RESEARCH WITH ALOS INTERFEROMETRY

PI-114 and CVST-21

David Sandwell⁽¹⁾, Yuri Fialko⁽¹⁾, Rob Mellors⁽²⁾, Meng Wei⁽¹⁾, Xiaopeng Tong⁽¹⁾

⁽¹⁾University of California at San Diego, La Jolla, CA, USA,
dsandwell@ucsd.edu, yfialko@ucsd.edu, mwei@whoi.edu, xitong@ucsd.edu

⁽²⁾San Diego State University, San Diego, CA, USA,
now at Lawrence Livermore National Laboratory, Livermore, CA, USA mellors1@llnl.gov

1. ABSTRACT

ALOS PALSAR is the first interferometric SAR mission with the ability to globally image (including vegetated areas) crustal deformation associated with earthquakes and volcanoes [1],[2]. We call it the "earthquake machine" because the instrument, spacecraft, and mission managers have captured the deformation signals of all major events since the satellite was launched in 2006. Our investigation using ALOS PALSAR had two main components.

First we developed algorithms and software to exploit the new modes of operation. We were perhaps the first group, outside of Japan, to: (1) create an interferogram with FBS to FBS L1.0 data [3]; (2) create mixed-mode FBD to FBS interferograms [4]; (3) interpolate the state vectors to verify better than 10 cm orbital accuracy [4]; (4) show the phase noise (in mm) for PALSAR is only 1.6 times worse than the phase noise at C-band even though the wavelength is 4 times longer [4]; (5) demonstrate the expected improved temporal correlation properties of L-band with respect to C-band [5]; and (6) develop the ability to create ScanSAR to ScanSAR interferograms as well as ScanSAR to FBD-mode interferograms [6]. We also discovered, as did our Japanese colleagues, that ionospheric waves with 20-40 km wavelength cause phase distortions as large as 20 cm that add significant noise to interferograms [6]. We were unable to correct these phase distortions using GPS-derived ionospheric models because they have insufficient spatial resolution to capture even the 40-km length scales. Since our algorithms, software, and funding (NASA and NSF) are independent of JAXA, our group provides an independent check of the strengths and weaknesses of ALOS-PALSAR.

The second main aspect of our investigation was to use these new InSAR data to image crustal deformation associated with: volcanic inflation at Kilauea, Hawaii [4],[7],[8]; the major deformation and decorrelation from the M7.9 Wenchuan, China earthquake [6]; the widespread deformation from the M8.8 Maule, Chile earthquake [9]; and most recently the deformation and liquefaction from the M7.2 El Major-Cucapah earthquake just south of the US-Mexico border in the Mexicali valley [10],[11],[12].

We have been less successful at using stacks of ALOS interferograms to image the interseismic crustal deformation along the San Andreas Fault system (SAF's). The typical spacing of continuously-operating GPS-receivers surrounding this fault system is 10 km so any new information from interferometry must capture deformation at smaller scales [13]. We expect the amplitudes of these short-wavelength signals to be 1 to 5 mm/yr. There are two reasons why ALOS has not adequately captured these signals. First the interferometric baseline of ALOS drifts by 5 km over a 1.9 year timescale so we are only now beginning to have short spatial baseline and long temporal baseline pairs needed to image the mm-scale deformation rates. Second, ALOS has not collected much PALSAR data on descending (daytime) tracks that have the optimal geometry for observing strike-slip motion of the SAF's. As the ALOS mission moves into its 6 year of data collection, the number of long temporal baseline interferograms is rapidly increasing and we expect significant interseismic findings over the next few years.

During our investigation we have participated in 8 ALOS PI meetings and have presented our results at 3 IGARSS meetings, 3 AGU meetings, 5 SCEC meetings, 3 EarthScope meetings and at least 6 invited talks at USC, Ohio State, Kyoto-DPRI, Stanford, UCSB, and UCR. Our group has published 8 papers in refereed journals. The remainder of this report describes the main findings from these publications.

One of the most important aspects of the scientific use of ALOS PALSAR data is open access to large quantities. We are grateful to JAXA for supplying 50 scenes/yr from the AUIG site for our cal/val investigation [14]. We were also allocated 50 scenes/year from the ASF AADN [15]. However, these 50 scene allocations are insufficient for this type of crustal deformation research since each study discussed below required the analysis of between 50 and 200 scenes. The bulk of these data were obtained from the ASF DAAC through the L1 data pool [16] that was supported with funds from NASA, NSF, and USGS. Moving data from JAXA to the AADN to the DAAC and finally into the L1-pool is sometimes slow and error prone so having access to the 50 scenes/yr at the AUIG site was a tremendous asset. The AUIG site contains all the

PALSAR data and it is usually available, with precise orbits, within 2 days after acquisition.

2. INTRODUCTION

This final report combines the findings of two investigations where Sandwell was the PI. The first investigation is PI-114 *Western North America Crustal Dynamics Research: WInSAR Consortium* and the second is CVST-21 *ALOS Cal/Val Support at University of California San Diego: Radar Corner Reflectors for Interferometric Phase Assessment*. Since they are related topics we decided to combine the final reports. Also note that the original investigation PI-114 had 45 co-investigators who represented the membership of WInSAR at the time the ALOS proposals were written. One of the main tasks of this WInSAR investigation was to provide JAXA with a priority list of data acquisitions to serve the needs of this large group of US investigators. The 50-scene allocation for the WInSAR group was, of course, insufficient to achieve the research objectives so WInSAR members helped to organize, and justify funding for, a large pool of PALSAR data (currently ~50,000 scenes) housed at the ASF DAAC. There will be a second final report for PI-114 submitted to JAXA representing the results of the larger WInSAR membership. This will be written by the current WInSAR leadership (Eric Fielding, chair). The final report presented next will summarize only the research findings and publications of the authors listed above.

2.1 Summary of proposed research - CVST-21

We installed three radar corner reflectors at Pinon Flat Observatory located between the San Andreas and San Jacinto Faults to support the radiometric, geometric, and interferometric assessment of PALSAR (Fig. 1.). These are permanent installations designed to remain in place for the lifetime of the ALOS mission and beyond. The precise locations of the reflectors and their radiometric design are available to any investigator for research. Each year we will visit the site and make repairs as necessary.

2.2 Summary of proposed research - PI-114

The western part of North America is the focus of intensive scientific research into a variety of plate boundary processes including earthquakes, volcanism, mountain building, and micro-plate tectonics. We proposed to use ALOS PALSAR data, with its unique L-band capabilities, for the following:

- Monitor strain accumulation and release along the North American/Pacific Plate Boundary with an emphasis on the San Andreas Fault Zone.
- Monitor the deformation of volcanic systems in the western US.
- Monitor crustal deformations at selected sites in the Basin and Range province and along the Baja California peninsula.

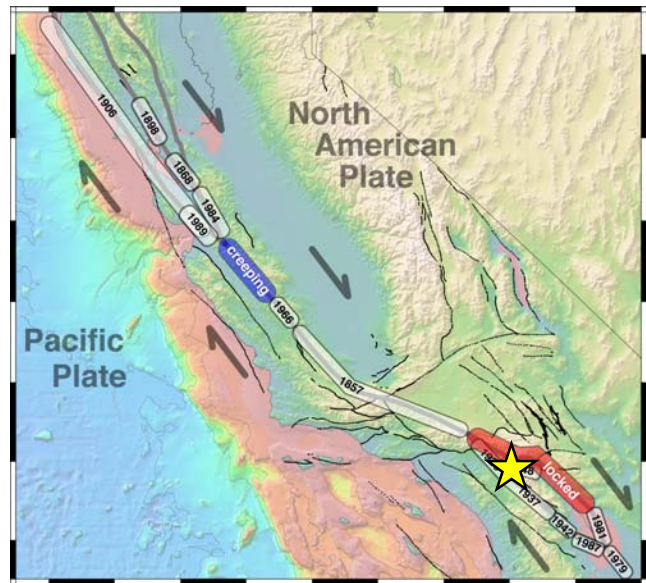


Fig. 1 The major sections of the San Andreas Fault zone undergo repeated earthquake activity except along the creeping section where the plates slide smoothly at all depths. Recent major earthquakes are dominated by the 1857 Fort Tejon Earthquake (M7.9) and the 1906 San Francisco Earthquake (M8.3). The southernmost locked section of the San Andreas Fault has not experienced a major earthquake in at least 300 years. The next event along this section should release more than 7 m of accumulated slip; typically large California earthquakes have a maximum slip of 6 m. Pinon Flat Observatory (yellow star) hosts a wide array of geodetic and seismic instrumentation including three large radar corner reflectors.

2.3 Research Objectives

Our proposed tasks and objectives follow:

- Modify existing InSAR processing algorithms to accommodate PALSAR data for change detection and DEM generation.
- Work with the ALOS team to schedule PALSAR data acquisitions over western North America. This will be done in co-ordination with the Alaska Satellite Facility (ASF).
- Compare L-band PALSAR-derived interferograms with C-band interferograms from ERS/Envisat as well as GPS measurements.
- Reduce the errors in PALSAR interferograms by modeling ionospheric and atmospheric artifacts.
- Publish and present scientific results in journals, scientific meetings, and at ALOS team meetings.

3. FINAL REPORT

This final report consists of a list of publications where ALOS PALSAR data were used followed by the significant findings of each publication.

3.1. Algorithms and Software Development - GMTSAR

Sandwell, D., R. Mellors, X. Tong, M. Wei, and P. Wessel, *GMTSAR: An InSAR Processing System Based on Generic Mapping Tools*, (software and documentation freely available at <http://topex.ucsd.edu/gmtsar>).

GMTSAR is an open source (GNU General Public License) InSAR processing system designed for users familiar with Generic Mapping Tools (GMT). The code is written in C and will compile on any computer where GMT and NETCDF are installed. The system has three main components: 1) a preprocessor for each satellite data type (e.g., ERS, Envisat, and ALOS) to convert the native format and orbital information into a generic format; 2) an InSAR processor to focus and align stacks of images, map topography into phase, and form the complex interferogram; 3) a postprocessor, mostly based on GMT, to filter the interferogram and construct interferometric products of phase, coherence, phase gradient, and line-of-sight displacement in both radar and geographic coordinates. GMT is used to display all the products as postscript files and kml-images for Google Earth. A set of C-shell scripts has been developed for standard 2-pass processing as well as image alignment for stacking and time series. ScanSAR processing is also possible but requires a knowledgeable user.

One of the key contributions of this software related to ALOS-PALSAR is a suite of pre-processing tools that will ingest L1.0 PALSAR data in either the AUIG or ERSDAC format and create data files that are compatible with either GMTSAR or ROI_PAC. All of this software as well as installation instructions and sample data sets are available at <http://topex.ucsd.edu/gmtsar>. An example interferogram is shown in Fig. 2.

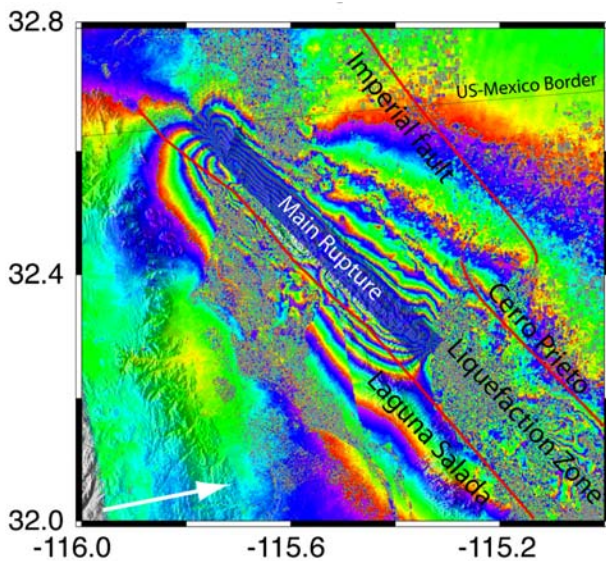


Fig. 2 ALOS interferograms processed with GMTSAR shows the co-seismic deformation of the Mw 7.2 April

4th Baja Earthquake. The rupture did not occur on any of the three main faults of the region, Imperial, Cerro Prieto, or Laguna Salada (red lines). Fault scarps of the main rupture are evident in the Cucapah mountains (blue shaded area). The interferograms are decorrelated in the liquefaction zone, which is bounded by the Cerro Prieto and Laguna Salada Faults.

3.2. Geometric Calibration of PALSAR

We tested the geolocation accuracy of PALSAR using 3 radar corner reflectors installed at Pinon Flat Observatory (Fig. 2 and Table 1). The positions of the corner reflectors are accurately measured using GPS. The orbits ALOS are determined to an accuracy of better than 30 cm and perhaps as good as 5 cm. The near range and timing of the satellite are provided with the data and should have sub-meter accuracy. Using this information one can predict the range and azimuth pixel where the bright radar reflection should appear in the image. We then focus each SAR image and locate the position of the radar reflectors as bright spots. This is done by eye to an accuracy of about 1 pixel in range and about 2 pixels in azimuth. The difference between the image-based coordinate and the orbital-based coordinate provides an estimate of the overall accuracy of the system.



Fig. 3 One of the 2.4 m radar corner reflectors at Pinon Flat Observatory installed in 1998. This arid region at an elevation of 1200 m is relatively flat with a surface of decomposed granite sparsely covered by bush and grass. Three radar corner reflectors are oriented to reflect energy from ascending (A1) and descending (D1 and D2) ALOS passes.

Table 1. Coordinates of Radar Reflectors

	lat	lon	height	azimuth
A1	33.612246	-116.456768	1258.990	257.5°
D1	33.612253	-116.457893	1257.544	102.5°
D2	33.607373	-116.451836	1254.537	102.5°

Latitude and longitude in decimal degrees and elevation in meters relative to the WGS-84 co-ordinate system and ellipsoid. The survey point is the apex (lowest corner) of each reflector.

We performed this analysis on all ALOS data available (27 points, Table 2). The mean differences are relatively small in both range (-1.2 +/- 0.6) and azimuth (0.6 +/- 1.1) so no biases have been included in the software for ALOS. The mean difference in range could be due to the path delay through the ionosphere. Based on this analysis we conclude that ground control is not needed for InSAR processing and orbital-based image alignment should be accurate to better than about 15 m in range and 10 m in azimuth.

Table 2. Comparison between ALOS image and orbit for Pinon corner reflectors.

NAME	Ri-Ro	Ai-Ao
ALPSRP022200660	-2.0	0.0
ALPSRP028910660	-2.1	0.0
ALPSRP035620660	-0.1	0.8
ALPSRP042330660	-2.3	2.2
ALPSRP049040660	-1.7	0.2
ALPSRP055750660	-1.9	0.8
ALPSRP062460660	-1.7	1.0
ALPSRP075880660	-0.7	2.0
ALPSRP082590660	-0.6	0.0
ALPSRP089300660	-0.6	-1.0
ALPSRP096010660	-1.0	1.0
ALPSRP109430660	-0.9	2.0
ALPSRP116140660	-0.5	0.0
ALPSRP122850660	-0.7	2.0
ALPSRP129560660	-1.1	2.0
ALPSRP136270660	-1.1	0.0
ALPSRP142980660	-1.5	0.0
ALPSRP149690660	-1.7	-2.0
ALPSRP156400660	-1.1	-1.0
ALPSRP163110660	-0.9	0.0
ALPSRP183240660	-1.3	1.0
ALPSRP189950660	-1.1	0.0
ALPSRP196660660	-1.1	0.0
ALPSRP210080660	-2.5	1.0
ALPSRP223500660	-1.8	1.0
ALPSRP230210660	-0.3	2.0
ALPSRP236920660	-1.0	0.0
mean	-1.2	0.6
rms	0.6	1.1

Ri/Ai - range/azimuth from image
 Ro/Ao - range/azimuth from orbit

3.3 Comparison of L-band PALSAR interferograms with C-band interferograms

Sandwell, D. T., D. Myer, R. Mellors, M. Shimada, B. Brooks, and J. Foster, Accuracy and resolution of ALOS interferometry: Vector deformation maps of the Father's Day Intrusion at Kilauea, IEEE Trans. Geosciences and Remote Sensing, 46, 3524-3534, 2008.

We assess the spatial resolution and phase noise of interferograms made from L-band ALOS SAR data and compare these results with corresponding C-band measurements from ERS. Based on cross-spectral analysis of phase gradients we find that the spatial resolution of ALOS interferograms is 1.3 times better than ERS interferograms. The phase noise of ALOS (i.e., line-of-sight (LOS) precision in the 100 m to 5000 m wavelength band) is 1.6 times worse than ERS (3.3 mm vs. 2.1 mm). In both cases the largest source of error is tropospheric phase delay. Vector deformation maps associated with the June 17, 2007 (Father's day) intrusion along the east rift zone of the Kilauea volcano were recovered using just 4 ALOS SAR images from two look directions (Fig. 4.). Comparisons with deformation vectors from 19 continuous GPS sites show rms line-of-site precision of 14 mm and an rms azimuth precision (flight direction) of 71 mm. This azimuth precision is at least 4 times better than corresponding measurements

made at C-band. Phase coherence is high even in heavily vegetated areas in agreement with previous results. This improved coherence combined with similar or better accuracy and resolution suggests that L-band ALOS will outperform C-band ERS in the recovery of slow crustal deformation.

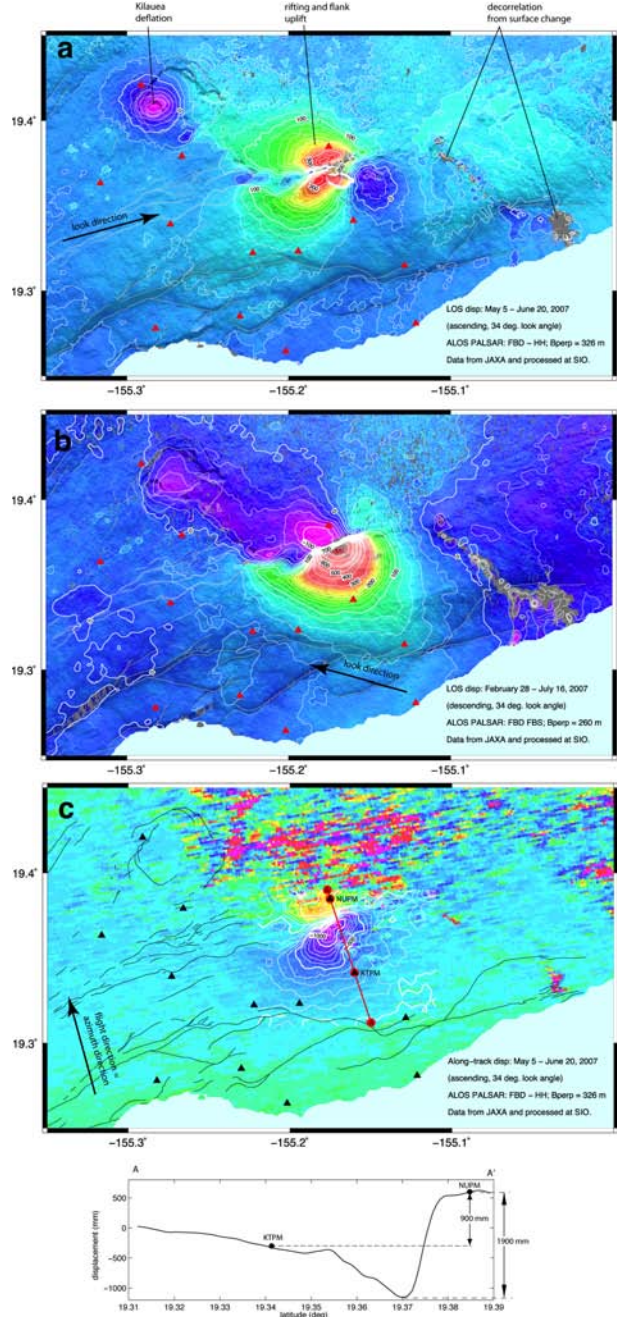


Fig. 4 (a) Radar interferogram constructed from ALOS PALSAR acquisitions on May 5 and June 20 (day 171, 8:52 GMT). This time period spans most of the “Father's Day” (June 17-20) rift event. These data were acquired in the fine beam dual polarization mode (FBD-HH, 14 MHz). Correlation is high even in forested areas and the phase was unwrapped and scaled to line-of-sight millimeters (LOS). The radar look direction is from the WSW and 34° from vertical.

GPS receivers with continuous vector measurements are marked by red triangles. (b) Radar interferogram constructed from ALOS PALSAR acquisitions on Feb 28 and July 16 (8:52 GMT). This time period spans the “Fathers Day” rift event. These data were acquired at two modes. The Feb 28 acquisition was FDB-HH (14 MHz) while the July 16 acquisition was FBS (28 MHz). The raw FDB data were interpolated to the higher FBS sampling rate. The radar look direction is from the ESE and 34° from vertical. (c) Crustal displacement in the flight direction from ALOS PALSAR acquisitions on May 5 and June 20 (day 171, 8:52 GMT). Displacements derived from cross correlation of image patches and scaled to mm. This component of displacement is perpendicular to the LOS displacement and also about 5 times less accurate. GPS receivers with continuous vector measurements are marked by black triangles. A displacement profile extracted along the line A-A’ shows excellent agreement with the baseline change between GPS sites NUPM and KTPM. This third component reveals a peak surface separation across the rift zone of 1.86 m, which is not fully captured (0.90 m) by the widely spaced GPS measurements. GPS data can be found at <http://www.soest.hawaii.edu/pgf/SEQ/>.

3.4 Volcanic Processes at Hawaii

Brooks, A. B., J. Foster, D. Sandwell, C. Wolfe, P. Okubo, M. Poland, and D. Myer, *Magmatically Triggered Slow-Slip at Kilauea Volcano, Hawaii, Nature*, 321, 2008.

Myer, D., D. Sandwell, B. Brooks, J. Foster, and M. Shimada, *Inflation along Kilauea's southwest rift zone in 2006, Journal of Volcanology and Geothermal Research*, 177, p. 418-424, 2008.

We report on InSAR and GPS results showing the first crustal inflation along the southwest rift zone (SWRZ) at Kilauea volcano in over 30 years. Two independent interferograms (May 2 – August 2, 2006 and June 22 – Nov 7, 2006) from the ALOS PALSAR instrument reveal domal uplift located southwest of the main caldera. The uplift is bounded on the northeast by the caldera and follows the southwest rift zone for about 12 km. It is approximately 8 km wide. We use data derived from permanent GPS stations to calibrate the InSAR displacement data and estimate uplift of 7.7 cm during the first interferogram and 8.9 cm during the second with line-of-sight volumes of $2.8 \times 10^6 \text{ m}^3$ and $3.0 \times 10^6 \text{ m}^3$ respectively. The earthquake record for the periods before, during, and after inflation shows that a swarm of shallow earthquakes ($z < 5 \text{ km}$) signaled the beginning of the uplift and that elevated levels of shallow seismicity along the rift zones occurred throughout the uplift period. GPS data indicate that the inflation occurred steadily over nine months between mid-January and mid-October, 2006 making injection of a sill unlikely. We attribute the inflation to decompression of a shallow ductile area under

the SWRZ.

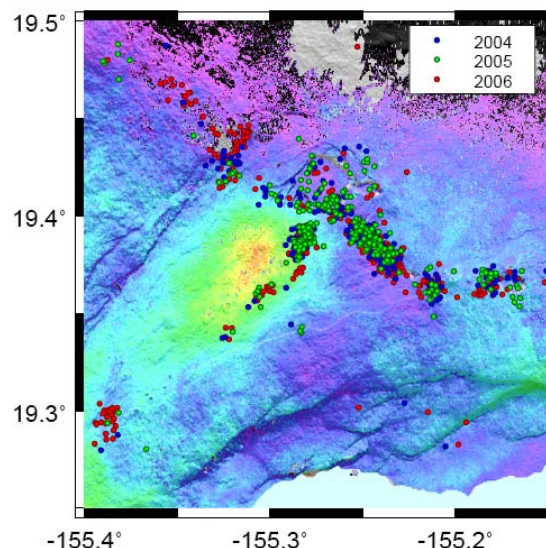


Fig. 5 Locations of shallow ($z \leq 5 \text{ km}$) earthquakes with magnitude ≥ 1.5 from the HVO catalog superimposed on InSAR displacement for scene T294. The earthquakes cluster in the main caldera (center of the image) and along the east and southwest rift zones for all three years. No significant change in spatial distribution is observed for 2006, the year of the uplift shown in the InSAR. Thin white lines indicate previously mapped faults, and faint shading is from topography layered underneath the displacement scene.

3.5 Large-Scale Earthquake Studies: The Mw 7.9, 2008 Wenchuan, China Earthquake - ScanSAR Interferometry

Tong, X., D. T. Sandwell, and Y. Fialko, *Coseismic Slip Model of the 2008 Wenchuan Earthquake Derived From Joint Inversion of InSAR, GPS and Field Data, J. Geophys. Res.*, 115, B04314, doi:10.1029/2009JB006625, 2010.

We derived a coseismic slip model for the M7.9 2008 Wenchuan earthquake based on radar line of sight displacements from ALOS interferograms, GPS vectors, and geologic field data. The surface rupture of the Wenchuan earthquake extended over 270 km from the epicenter toward the northeast along Longmen Shan thrust belt, on the steep margin of the Tibetan plateau. Available InSAR data provided a nearly complete coverage of the surface deformation along both ascending (fine beam mode) and descending orbits (ScanSAR to ScanSAR mode Fig. 6). The earthquake was modeled using 4 subfaults with variable geometry and dip to capture the simultaneous rupture of both the Beichuan and the Pengguan fault (Fig. 7). We inverted the InSAR and GPS data using a non-negative least squares (NNLS) algorithm incorporating the scarp height data as an additional inequality constraint. The coseismic rupture model of the 2008 Wenchuan earthquake, which is mainly based on

space geodetic observations, suggests that most of the moment release was limited to the shallow part of the crust (depth less than 10 km). We didn't find any "shallow slip deficit" in the slip-depth distribution of this mixed-mechanism earthquake. Aftershocks were primarily distributed below the section of the fault that ruptured coseismically. This coseismic rupture model will be used in forward models of postseismic deformation to provide insights on mechanisms of postseismic relaxation, the effective rheology of the lower crust and upper mantle, stress transfer, earthquake triggering and future seismic hazard in the area.

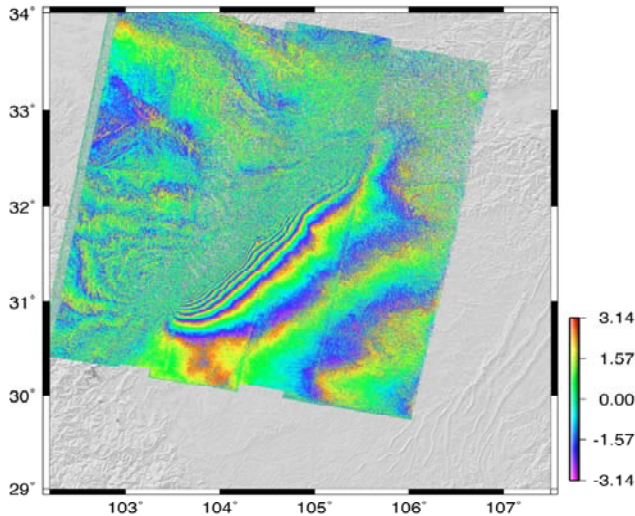


Fig. 6 Descending ScanSAR mode interferograms after trend removal (11.8 cm per fringe). Each scene of the interferogram consists of 5 sub-swaths across look direction. The decorrelation in the mountainous area is probably due to long baseline (920m).

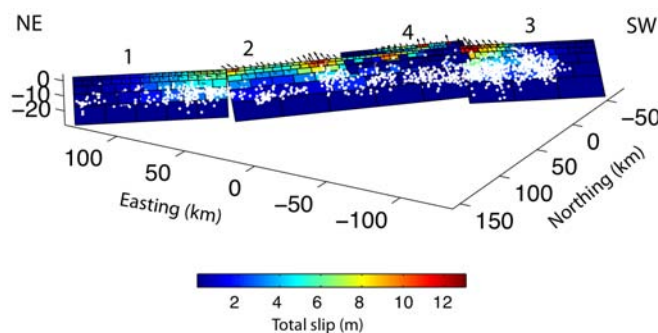


Fig. 7 Coseismic slip model in 3D view. The white dots are the aftershocks from double difference relocation.

3.5 Large-Scale Earthquake Studies: Mw, 8.8, 2010 Maule Chile Earthquake - ScanSAR Interferometry

Tong, X., D. Sandwell, K. Luttrell, B. Brooks, M. Bevis, M. Shimada, J. Foster, R. Smalley Jr., H. Parra, J. C. Báez Soto, M. Blanco, E. Kendrick, J. Genrich, and D. J. Caccamise II, *The 2010 Maule, Chile earthquake: Downdip*

rupture limit revealed by space geodesy, Geophys. Res. Lett., 37, L24311, doi:10.1029/2010GL045805, 2010.

Radar interferometry from the ALOS satellite captured the coseismic ground deformation associated with the 2010 Mw 8.8 Maule, Chile earthquake. The ALOS interferograms reveal a sharp transition in fringe pattern at ~150 km from the trench axis that is diagnostic of the downdip rupture limit of the Maule earthquake. An elastic dislocation model based on ascending and descending ALOS interferograms and 13 near-field 3-component GPS measurements reveals that the coseismic slip decreases more or less linearly from a maximum of 17 m (along-strike average of 6.5 m) at 18 km depth to near zero at 43-48 km depth, quantitatively indicating the downdip limit of the seismogenic zone. The depth at which slip drops to near zero appears to be at the intersection of the subducting plate with the continental Moho. Our model also suggests that the depth where coseismic slip vanishes is nearly uniform along the strike direction for a rupture length of ~600 km. The average coseismic slip vector and the interseismic velocity vector are not parallel, which can be interpreted as a deficit in strike-slip moment release.

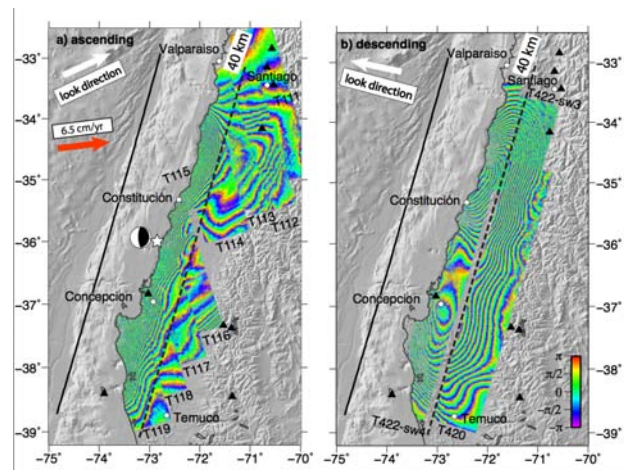


Fig. 8 Nine tracks of ascending interferograms (FBS-FBS mode) and two tracks of descending interferograms (two subswaths of ScanSAR-ScanSAR mode and ScanSAR-FBS mode, and one track of FBS-FBS mode). The bold white arrow shows the horizontal component of the LOS direction. The nominal look angle from the vertical is 34°. The wrapped phase ($-\pi$ to π) corresponds a range change of 11.8 cm per cycle). The white star indicates the earthquake epicenter. The black triangles show the locations of the 13 GPS sites used in the inversion (4 sites are outside of the boundaries). Solid black line shows the surface trace of the simplified fault model and the dashed black line marks the 40-km depth position of the fault for a 15° dip angle. The bold red arrow shows the interseismic convergence vector.

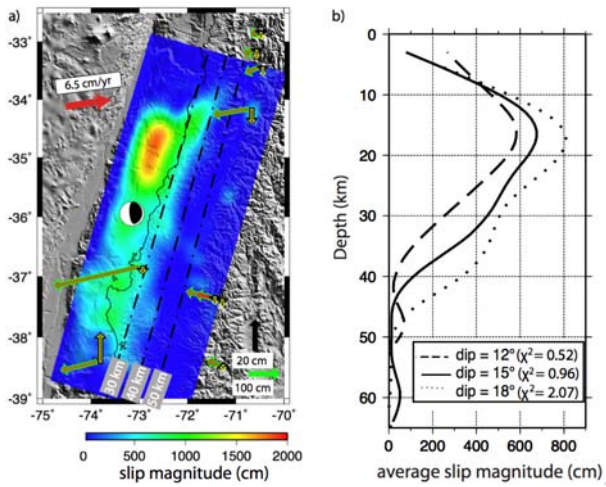


Fig. 9 a) Coseismic slip model along a 15° dipping fault plane over shaded topography in Mercator projection. Dashed lines show contours of fault depth. The fat green and black arrows show the observed horizontal and vertical displacement of the GPS vectors respectively and the narrow red and yellow arrows show the predicted horizontal and vertical displacement. **b)** Averaged slip versus depth for different dip angles.

3.7 Interseismic Deformation on the San Andreas Fault System

Wei, M., and D. T. Sandwell, Decorrelation of ALOS and ERS interferometry over vegetated areas in California, IEEE Geosciences and Remote Sensing, 10.1109/TGRS.2010.2043442, 2010.

Temporal decorrelation is one of the main limitations for recovering interseismic deformation along the San Andreas Fault system using interferometric Synthetic Aperture Radar. To assess the improved correlation properties of L-band with respect to C-band, we analyzed L-band ALOS interferograms having a range of temporal and spatial baselines over three vegetated areas in California and compared them with corresponding C-band ERS interferograms. Over the highly vegetated Northern California forests (Fig. 10) in the Coast Range area, ALOS remains remarkably well correlated over a two-year period, while an ERS interferogram with a similar temporal and spatial baseline lost correlation (< 0.2). In Central California near Parkfield, we found a similar pattern in decorrelation behavior, which enabled the recovery of a fault creep and a local uplifting signal at L-band that was not apparent at C-band. In the Imperial Valley of Southern California, both ALOS and ERS have low correlation over farmlands. Surprisingly, ALOS has lower correlation over some sandy surfaces than ERS. In general L-band interferograms with similar seasonal acquisitions have higher correlation than those with dissimilar season. For both L- and C-band, correlation over vegetated areas decreases with time for intervals less than 1 year and then remains relatively constant at longer time intervals. Overall these results suggest that L-band

interferograms will reveal near-fault interseismic deformation once sufficient data become available.

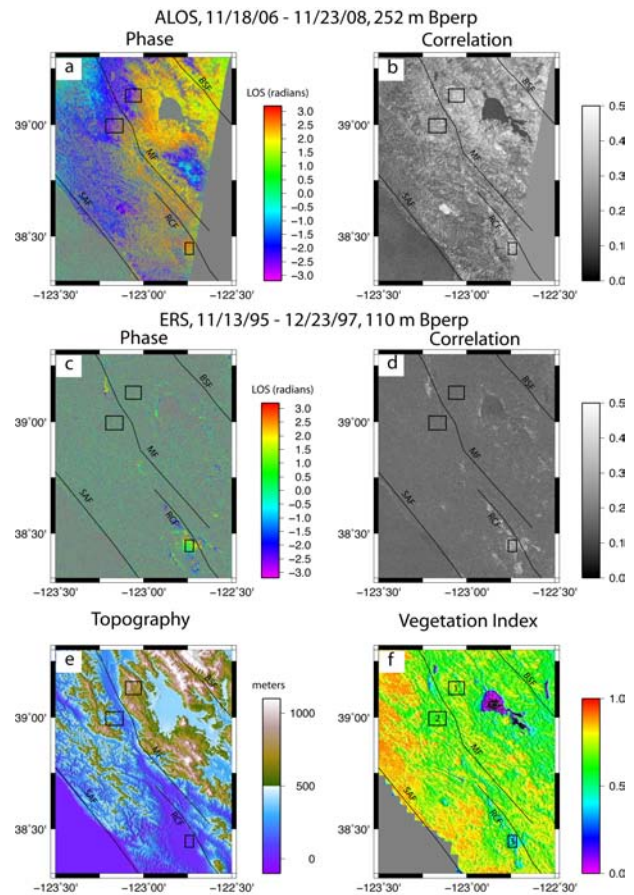


Fig. 10 Comparison between ERS and ALOS interferograms in the Coast Range area in Northern California. Each interferogram spans approximately 2 years but the ERS-interferogram has poor correlation while the L-band interferogram has adequate correlation.

Wei, M., D. T. Sandwell, and B. Smith-Konter, Optimal Combination of InSAR and GPS for Measuring Interseismic Crustal Deformation, J. Adv. in Space Res. doi:10.1016/j.asr.2010.03.013, 2010.

High spatial resolution measurements of interseismic deformation along major faults are critical for understanding the earthquake cycle and for earthquake hazard assessment. Based on the spacing of GPS stations in California and the characteristics of interseismic signal and noise using InSAR, a remove/filter/restore technique is proposed to optimally combine GPS and InSAR data to measure interseismic crustal deformation; GPS measurements, combined with a dislocation model, are used to constrain the longer wavelengths (> 40 km) while InSAR measurements provide the shorter wavelength information. The method is tested in three areas, the Salton Sea area, the Creeping section (Fig. 11), and the Mojave/Big Bend section of the San Andreas Fault, with both ERS and ALOS data. The contribution of InSAR for

recovering the short wavelength signal is demonstrated. The results show a zone of uplift to the west of the creeping section of the SAF and an area of subsidence near city of Lancaster, CA. The InSAR data provide an improved fit to the GPS data of 26%, 11% and 0% in the Salton Sea area the Creeping section, and the Mojave/Big Bend area, respectively. Our analysis suggests that ALOS interferograms will provide a major contribution toward measuring interseismic deformation after collecting data for 5 years in orbit.

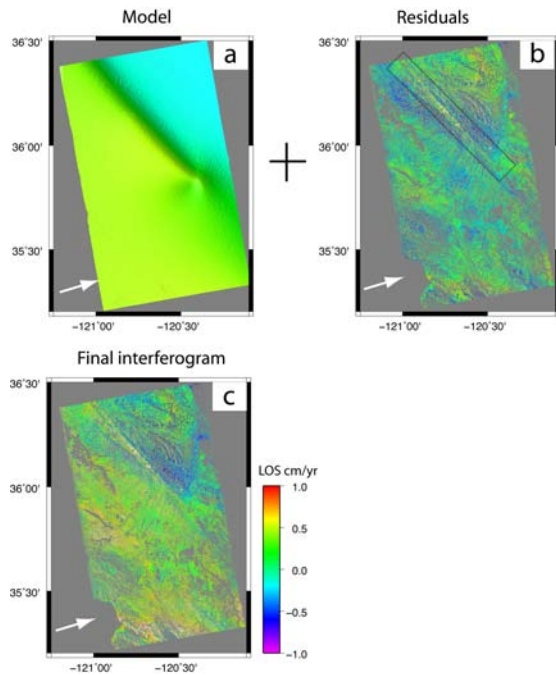


Fig. 11 Interferograms using the filtering method along the Creeping section of the SAF (a) Base model constrained by the GPS data. (b) Stacked residual interferograms after applying the filtering method. (c) The final interferogram is the sum of base model and the residual interferogram. Thin grey solid line shows the main fault trace of the San Andreas Fault. White arrow indicates the satellite look direction.

3.8 Main Rupture and Triggered Slip from the M7.2 El Mayor-Cucapah Earthquake

Wei, M., and D. Sandwell, The M7.2 El Major-Cucapah Earthquake in Baja California: Extensive Liquefaction Identified in ALOS InSAR Data, Alaska Satellite Facility News & Notes, v. 6:4, Fall 2010.

A magnitude 7.2 earthquake struck Northern Baja California at 3:40 p.m. Pacific Time on Easter Sunday, April 4th, 2010. The epicenter was located in Mexico about 63 km southeast of Calexico, CA (Fig. 12). This earthquake temblor was widely felt through southern California, and some felt reports came in from more distant locations such as Santa Barbara, California, and Las Vegas, Nevada. This earthquake is the largest

earthquake in this region in 18 years, after the 1992 M7.3 Landers earthquake.

The 120 km long bilateral rupture lasted for more than 45 seconds causing extensive damage to buildings in Calexico (US) and Mexicali (Mexico). According to the Assistant Director of Civil Protection in Tijuana, at least two people died and more than 100 were injured in Mexicali (CNN report). The entire city of Mexicali, a large metropolitan area and the capital of Mexico's Baja California state, lost power as a result of this earthquake. The most significant damage occurred in the agricultural areas of the Colorado River Delta southeast of the main rupture, where over an area of 200 square kilometers irrigation systems had to be shut down, and ~35,000 people were displaced from their damaged homes and are now living in tent cities. The extent of damage to the agricultural areas due to liquefaction is far worse than initially reported.

The mainshock rupture, as revealed by aftershocks and radar interferometry, occurred on largely unmapped faults in the Cucapa Mountains and beneath the Colorado River delta (Fig. 13). Two of the highest slip rate faults of the San Andreas system, the Imperial and Cerro Prieto Faults (35-40 mm/yr), are within this general area. The ALOS InSAR data collected on April 17 along the track 211 and 533, on May 4 along the track 212 and on May 16 along the track 532 show two main features (Fig. 13): 1) The main rupture in the Sierra El Cucapa consists of at least two concentrations of right-lateral and east-side down normal faulting. Interferograms are decorrelated in the steep mountain areas where the combination of strong ground acceleration and steep slope produced major surface slides. 2) The southwest extension of the rupture goes beneath the agricultural area of the Colorado River Delta where the aqueduct system was destroyed. More importantly, the ALOS interferogram reveals the full extent of the 18 km by 60 km liquefaction zone. It is bounded on the east by the Cerro Prieto fault and on the west by the Laguna Salada fault. Field observations show that the roads have undulations with vertical amplitudes of 20-50 cm and most of the concrete lined aqueducts are fractured. Interferograms are decorrelated over much of the area although azimuth offsets help to delineate the zone of deep slip.

In the first few weeks after the Easter Sunday earthquake, the scientific community gathered seismic and geodetic data sufficient to map the rupture plane as well as to assess areas of highest ground acceleration. Repeat-pass radar interferometry (InSAR) data was a critical component of this effort providing cm-precision co-seismic deformation maps over a 100 km by 400 km region. Field geologists use these maps as a reconnaissance tool for mapping the rupture. The ALOS L1 data pool at the Alaska Satellite Facility (ASF) was a critical resource needed for rapid response to this earthquake since it contained most of the pre-earthquake ALOS SAR images. ASF also worked in collaboration with Japan Aerospace Exploration

Agency (JAXA) to optimally schedule post earthquake acquisitions. The critical data were acquired on April 17, May 4 and May 16 along the ascending and descending tracks shown in Fig. 13. The interferograms show that the fault slipped both vertically, east side down, and horizontally, right lateral. More importantly, these maps also reveal details of the surface rupture and the extent of the liquefaction zone. A preliminary co-seismic model based on InSAR can be found at Professor Yuri Fialko's website at <http://igpp.ucsd.edu/~fialko/baja.html>.

While timely data access (24 hr) was available for the two April 17 ALOS acquisitions, access to later acquisitions, including the May 4 and May 16 acquisitions, were delayed by typically 2 weeks. This delay occurred because neither the ASF nor most of the scientific community has direct access to the AUIG archive in Japan where all ALOS data are acquired and archived. It is important to reduce this delay time, as rapid response to large earthquakes like this one is crucial for advancing scientific knowledge about the earthquake and to help mitigate seismic hazards within the community affected by the earthquake. Compared to the 2 weeks delay of attaining the ALOS data for this region, the data from European Satellite ENVISAT are accessible to the US scientific community through the Western North America InSAR Consortium (WINSAR) within ~1 week. The delay of the ALOS data for the 2010 Baja Earthquake shows the importance of a need for a closer collaboration between JAXA and ASF and the benefits of having a US InSAR satellite, such as DESDynI (planned to launch in 2017).

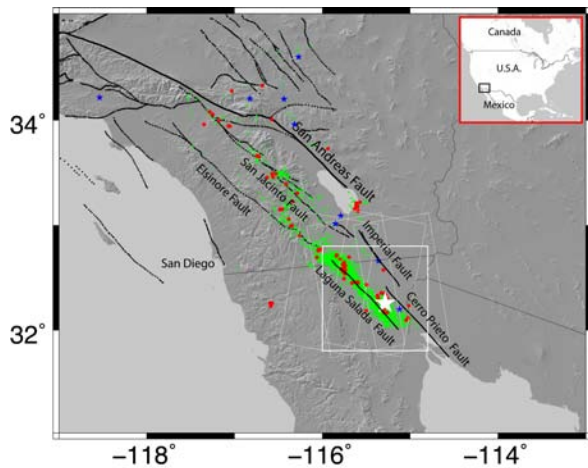


Fig. 12 Map of Southern California and Northern Baja California. Inset map shows the geographical relationship between our study region (box) and the USA and Mexico (labeled). In the main figure, bold black lines and black dotted lines represent major faults in the area. Blue stars are earthquakes of magnitude 6 or above since 1969. White star is the epicenter of the April 4th Baja earthquake. Red dots are earthquakes 1 day before and after the major event, April 3rd - April 5th, 2010. Green dots are earthquake's (magnitude > 1) within one month

after the mainshock event, April 5th – May 5th. Earthquake data is from the Southern California Earthquake Center. The white square box covers the extent of Fig. 2. The four tilting rectangular boxes are the areas of ALOS track T211, T212, T532 and T533.

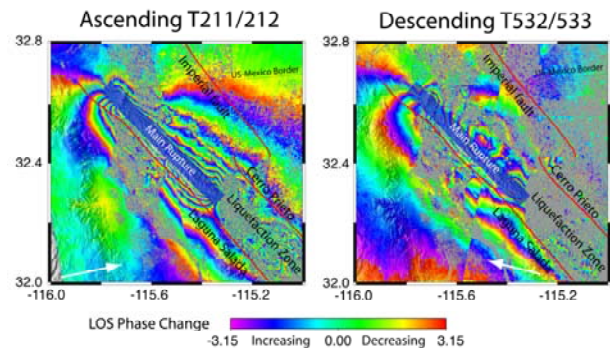


Fig. 13 ALOS interferograms show the co-seismic deformation of the Mw 7.2 April 4th Baja Earthquake. The left figure is from ascending tracks T211 and T212. The right figure is from descending track T532 and T533. Color change from cold to warm represents decreasing in range. The interpretation is that the fault is right lateral and with a vertical component of east side down. The rupture did not occur on any of the three main faults of the region, Imperial, Cerro Prieto, or Laguna Salada (red lines). Fault scarps of the main rupture are evident in the Cucapa mountains (blue shaded area). The interferograms are decorrelated in the liquefaction zone, which is bounded by the Cerro Prieto and Laguna Salada Faults.

Wei, M., D. Sandwell, Y. Fialko, and R. Bilham Slip on faults in the Imperial Valley triggered by the 4 April 2010 Mw 7.2 El Mayor-Cucapah earthquake revealed by InSAR *Geophys. Res. Lett.*, doi:10.1029/2010GL045235, in press, 2011.

Radar interferometry (InSAR) and field measurements reveal surface slip on multiple faults in the Imperial Valley triggered by the 2010 Baja M7.2 earthquake. Co-seismic offsets occurred on the San Andreas, Superstition Hills, Imperial, Elmore Ranch, Wienert, Coyote Creek, Elsinore, Yuha Wells, and several minor faults near the town of Ocotillo at the northern end of the mainshock rupture. We documented right-lateral slip (< 40 mm) on northwest trending faults and left-lateral slip (< 40 mm) on southwest trending faults. Slip occurred on 15-km- and 20-km-long segments of the San Andreas Fault in the Mecca Hills (≤ 50 mm) and Durmid Hill (≤ 10 mm) respectively, and 25 km of the Superstition Hills Fault (≤ 37 mm). Field measurements of slip on the Superstition Hills Fault agree with InSAR and creepmeter measurements to within a few millimeters (Fig. 14). Dislocation models of the InSAR data on the Superstition Hills Fault confirm that creep in this sequence, as in previous slip events, is confined to shallow depths (< 3 km).

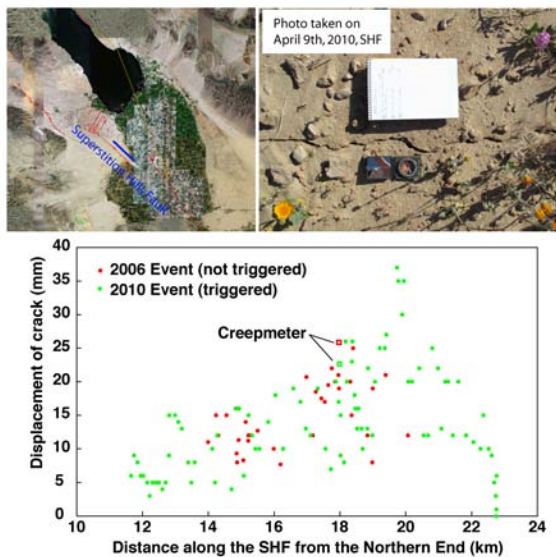


Fig. 14 Field measurements of triggered slip on the Superstition Hills fault for the 2006 and 2010 events.

4. CONCLUSIONS AND RECOMMENDATIONS

ALOS PALSAR is the premiere instrument for imaging major crustal dynamic events such as volcanic inflation and earthquakes.

Mixed mode interferometry, including ScanSAR to stripmode, is practical. The most difficult programming issue is related to changes in the pulse repetition frequency (PRF) both along and between passes. A fixed PRF for each mode, or subswath, would simplify processing and enlarge the number of interferometric pairs.

ScanSAR to ScanSAR interferometry provides wide area coverage and adequate spatial resolution but the bursts must have greater than 20% overlap to achieve phase coherence.

Over areas of moderate vegetation, L-band interferograms retain adequate phase coherence for time intervals of at least 2 years while C-band interferograms are decorrelated after only 6 months. This improved temporal correlation will enable InSAR imaging of interseismic deformation.

In accordance with theory, the ionospheric phase delay at L-band is 16 times greater than at C-band. Moreover, PALSAR has revealed smaller spatial scale ionospheric perturbations (20-40 km) that are not resolved by the best ionosphere models. Future L-band InSAR missions would benefit from routine dual-frequency operation to correct for ionospheric delay.

The next frontier of InSAR is the recovery of interseismic deformation, especially in areas of sparse GPS coverage. This will require large (>10) stacks of

long time span interferograms (1-2 years) to reduce the tropospheric and ionospheric phase perturbations. Extending the ALOS mission by 4 to 6 years will dramatically increase the number of interferometric pairs so recovery of interseismic deformation will be possible.

Strike-slip motion along the San Andreas Fault system results in small line-of-sight displacements for interferograms made from ascending tracks. More descending acquisitions are needed to better image the small-scale crustal deformation not resolved by the GPS array.

5. ACKNOWLEDGEMENTS

The ALOS PALSAR data were supplied by JAXA AUIG and the Alaska Satellite Facility and we thank the help desks at AUIG and ASF for their prompt response to data requests and corrections. We thank Craig Dobson, Eva Zanzerkia, and Daniel Dzurisin for their efforts in organizing and funding the ALOS-L1 data pool used in this analysis. This research was supported by the NASA Geodetic Imaging Program (NNX09AD12G) and the NSF Geophysics Program (EAR 0811772).

6. REFERENCES

- [1] M. Shimada, O. Isoguchi, T. Tadono, R. Higuchi, and K. Isono, "PALSAR CALVAL summary and update 2007," in Proc. IGARSS, Barcelona, Spain, 2007, pp. 3593–3596.
- [2] A. Rosenqvist, M. Shimada, N. Ito, and M. Watanabe, "ALOS PALSAR: A pathfinder mission for global-scale monitoring of the environment," IEEE Trans. Geosci. Remote Sens., vol. 45, no. 11, pp. 3307–3316, Nov. 2007.
- [3] Sandwell, D. and M. Wei, ALOS Interferometry, <http://topex.ucsd.edu/alos/>, August 18, 2006.
- [4] Sandwell, D. T., D. Myer, R. Mellors, M. Shimada, B. Brooks, and J. Foster, Accuracy and resolution of ALOS interferometry: Vector deformation maps of the Father's Day Intrusion at Kilauea, IEEE Trans. Geosciences and Remote Sensing, 46, 3524-3534, 2008.
- [5] Wei, M., and D. T. Sandwell, Decorrelation of ALOS and ERS interferometry over vegetated areas in California, IEEE Geosciences and Remote Sensing, 10.1109/TGRS.2010.2043442, 2010.
- [6] Tong, X., D. T. Sandwell, and Y. Fialko, Coseismic Slip Model of the 2008 Wenchuan Earthquake Derived From Joint Inversion of InSAR, GPS and Field Data, J. Geophys. Res., 115, B04314, doi:10.1029/2009JB006625, 2010.
- [7] Brooks, A. B., J. Foster, D. Sandwell, C. Wolfe, P. Okubo, M. Poland, and D. Myer, Magmatically Triggered Slow-Slip at Kilauea Volcano, Hawaii, Nature, 321, 2008.
- [8] Myer, D., D. Sandwell, B. Brooks, J. Foster, and M.

Shimada, Inflation along Kilauea's southwest rift zone in 2006, *Journal of Volcanology and Geothermal Research*, 177, p. 418-424, 2008.

- [9] Tong, X., D. Sandwell, K. Luttrell, B. Brooks, M. Bevis, M. Shimada, J. Foster, R. Smalley Jr., H. Parra, J. C. Báez Soto, M. Blanco, E. Kendrick, J. Genrich, and D. J. Caccamise II, The 2010 Maule, Chile earthquake: Downdip rupture limit revealed by space geodesy, *Geophys. Res. Lett.*, 37, L24311, doi:10.1029/2010GL045805, 2010.
- [10] Fialko, Y, A. Gonzalez, J. J. Gonzalez, S. Barbot, S. Leprince, D. T. Sandwell, D. C. Agnew, Static Rupture Model of the 2010 M7.2 El Mayor-Cucapah Earthquake from ALOS, ENVISAT, SPOT and GPS Data, Abstract T53B-2125 presented at 2010 Fall Meeting, AGU, San Francisco, CA, 13-17 Dec, 2010.
- [11] Wei, M., and D. Sandwell, The M7.2 El Major-Cucapah Earthquake in Baja California: Extensive Liquefaction Identified in ALOS InSAR Data, *Alaska Satellite Facility News & Notes*, v. 6:4, Fall 2010.
- [12] Wei, M., D. Sandwell, Y. Fialko, and R. Bilham Slip on faults in the Imperial Valley triggered by the 4 April 2010 Mw 7.2 El Mayor-Cucapah earthquake revealed by InSAR *Geophys. Res. Lett.*, doi:10.1029/2010GL045235, in press, 2011.
- [13] Wei, M., D. T. Sandwell, and B. Smith-Konter, Optimal Combination of InSAR and GPS for Measuring Interseismic Crustal Deformation, *J. Adv. in Space Res.* doi:10.1016/j.asr.2010.03.013, 2010.
- [14] <https://auig.eoc.jaxa.jp/auigs/top/TOP1000Init.do>
- [15] <https://ursa.aadn.alaska.edu/cgi-bin/login/guest/>
- [16] <https://ursa.asfdaac.alaska.edu/cgi-bin/login/>